

Prepared for Joe Michael's
special issue of IJCK
March 10, 2020

“Third-Body” Collision Parameters for Hydrocarbons, Alcohols, and Hydroperoxides and an Effective Internal Rotor Approach for Estimating Them

AHREN W. JASPER

Chemical Sciences and Engineering Division, Argonne National Laboratory, Lemont, IL 60439

ABSTRACT. Collision rate constants and third-body collision efficiencies are calculated for more than 300 alkanes, alcohols, and hydroperoxides, for the bath gases He, Ar, H₂, and N₂, and from 300 to 2000 K. The data set includes highly branched species and species with as many as 16 nonhydrogen atoms N , and it is analyzed to develop strategies for estimating collision properties more generally. Simple analytic formulas describing the Lennard–Jones collision parameters σ and ε are obtained for each of the three classes of systems as a function of N . Trends in the collision efficiency range parameter $\alpha = \langle \Delta E_d \rangle$ are more complicated, and a method is developed and validated for estimating α based on the numbers and types of internal rotors and oxygen-containing groups. Specifically, the approach maps the expected value of α for a branched alkane, alcohol, or hydroperoxide onto those for the corresponding normal (linear) series via an effective number of nonhydrogen atoms N_{eff} . The prescription for N_{eff} is based on counting internal rotor types and is shown to be insensitive to temperature and fairly insensitive to the identity of the bath gas. Together, these strategies allow for the ready estimation of the collision parameters σ , ε , and α so long as results for the associated linear series are available.

*Corresponding author. E-mail address: ajasper@anl.gov.

1. INTRODUCTION

Detailed chemical kinetic models are comprised of (nowadays, often quite extensive) parameter databases describing elementary reaction rates, thermochemistry, and transport [1–9]. The role of a priori theory as an independent source of information for populating these databases and for improving the models they reflect continues to increase [10–13].

Here, we consider a priori theoretical approaches for computing collision rate constants and efficiencies relevant to the prediction of transport properties [14–16] and pressure dependence in elementary kinetics [17–20]. These phenomena are controlled by so-called “third body” bath gas collisions, and we recently used trajectory-based collision parameters to compute diffusion coefficients [21] and pressure dependent kinetics [22] with accuracies comparable to those from experiment. Our predictive work benefitted from a long history of combustion-relevant trajectory studies of collisional energy transfer (see for example [23–32] and the recent review from Lendvay [33]) as well as quantum mechanical scattering predictions of transport properties [34–37], and it is similar to ongoing work from several groups (for example [38–41]).

Collisional activation is the dynamical bottleneck in the low-pressure limit of a unimolecular reaction, $A (+M) = B + C (+M)$, where the reaction rate $k_{0,M}[A][M]$ depends linearly on pressure. Chemical kinetics tabulations sometimes include $k_{0,M}$ for a reference bath gas (e.g., Ar) along with relative collision efficiencies (expressed as ratios of $k_{0,M}$) for other baths, but for many reactions this information is not available. More generally and despite some systematic experimental studies (for example [42–54]), it remains difficult to anticipate how collision efficiencies vary with the temperature and identity of the bath gas M as well as the size and chemical structure of the unimolecular reactant A.

We do know that the rate constants $k_{0,M}$ can vary significantly for different bath gases M and that their relative efficiencies are temperature dependent. As examples we highlight a few

experimental studies from Michael and co-workers. In a series of papers from the 1970s [42–44], $k_{0,M}$ was shown to vary by as much as factor of four even among the so-called “weak” colliders (e.g., $M = \text{He}, \text{Ar}, \text{Kr}, \text{H}_2, \text{N}_2, \text{O}_2$), while more recently [50] the important combustion reaction $\text{H} + \text{O}_2 (+M)$ was shown to be $\sim 25\times$ faster for the strong collider $M = \text{H}_2\text{O}$ than for $M = \text{Ar}$.

The goal of the present work is to use trajectory-based predictions of collisional energy transfer to develop rules for describing how the collision parameters that control $k_{0,M}$ depend on the size, composition, and structure of A. Specifically, we consider a total of 307 unimolecular reactants A with as many as 16 nonhydrogen (“heavy”) atoms N , including alcohols, hydroperoxides, and highly branched hydrocarbons, and the baths $M = \text{He}, \text{Ar}, \text{H}_2$, and N_2 .

The present work considerably extends our previous study [55] where 38 hydrocarbons with $N = 1$ to 8 were studied for seven baths, $M = \text{He}, \text{Ne}, \text{Ar}, \text{Kr}, \text{H}_2, \text{N}_2$, and O_2 . Collision parameters were found to be quite similar for $M = \text{Ar}$ and Kr and for N_2 and O_2 , and we therefore exclude Kr and O_2 from consideration here along with Ne , which is less commonly needed in combustion database compilations. Important baths like $M = \text{H}_2\text{O}$ and CO_2 are also not considered, as these baths require complex strategies for accurately representing their A + M interaction potentials that complicate the consideration of large numbers of systems [56].

The large data set generated here is analyzed to develop and validate simple expressions for estimating the Lennard–Jones collision parameters σ and ε as well as a commonly used measure of the collision efficiency $\alpha = \langle \Delta E_d \rangle$, which is the average energy transferred in deactivating collisions. We show that α can be reliably estimated using an “effective” number of nonhydrogen atoms N_{eff} , which is determined simply by counting the numbers and types of internal rotors (e.g., torsions) in A.

This paper is organized as follows. In Sec. 2, we briefly summarize the strategies used here for potential energy surface construction, for computing the Lennard–Jones parameters σ and ε , and for preparing and analyzing the trajectories used to compute α . We also outline a general automation strategy that enabled the more than 11 million trajectories that were needed for this work. Section 3 includes a brief test of our choice of molecular mechanics force field for describing A. Then, the systematic parameterization of N_{eff} is described using data for 1000 K and $M = \text{Ar}$. The resulting prescriptions for N_{eff} are subsequently tested and validated using the full data set, including data obtained at 300 and 2000 K and for $M = \text{He}, \text{H}_2, \text{and } \text{N}_2$. Section 4 is a conclusion.

2. THEORY

Potential energy surfaces. Potential energy surfaces (PESs) describing $A + M$ collisions are a prerequisite for predicting collision parameters, and we have previously used a simple transferable “separable and pairwise” approach for constructing them [57]. Similar approaches have a long history of use in trajectory studies of collisional energy transfer (for example [58–61]). Briefly, pairwise Buckingham ($\text{exp}/6$) interactions were parameterized against calculated ab initio interaction energies for a reference system ($\text{CH}_4 + M$). The resulting interaction parameters were assumed to be transferable to larger $\text{C}_x\text{H}_y + M$ systems, and the good accuracy of this assumption was demonstrated [55,56]. This approach greatly simplifies the consideration of large numbers of systems, as required here.

For $\text{C}_x\text{H}_y + \text{He}, \text{Ar}, \text{H}_2, \text{and } \text{N}_2$ and $\text{C}_x\text{H}_{2x+1}\text{OH} + \text{He}$ and Ar , we used our previously developed $\text{exp}/6$ parametrizations [56,57]. New $\text{exp}/6$ PESs were generated for this work to describe $\text{C}_x\text{H}_{2x+1}\text{OOH} + \text{He}$ and Ar using the same electronic structure theory, sampling, and fitting strategies that were used for alcohols in Ref. [56]. The new $\text{C}_x\text{H}_{2x+1}\text{OOH} + \text{He}$ and Ar

parameterizations and comparisons of the ab initio and fitted energies are included as supporting information. As noted in Ref. [56], the separable and pairwise exp/6 approach is not accurate when the interaction potential is too anisotropic, such as for alcohols and $M = N_2$. Therefore, diatomic baths were not considered here for any oxygenated species A.

In the present work, the species A are common organic molecules, and A + M collisions are always nonreactive. We therefore used molecular mechanics force fields for describing the intramolecular PES of A. Specifically, the Tinker software package [62] was used, and we tested three related force fields distributed with it: MM3 [63], AMBER [64], and OPLS [65]. A tight binding (TB) model for hydrocarbons was also tested [66]. As shown below, we find only small differences in the results obtained using the different force fields, and unless otherwise indicated the present results were obtained using MM3.

The Lennard–Jones parameters σ and ε . As described in a recent review [15], transport databases typically consist of pairs of Lennard–Jones parameters (the well depth ε and collision diameter σ) describing self-collisions (i.e., A + A collisions) for every species of interest. Combining rules are employed to generate the required binary (i.e., A + M) collision parameters (typically via geometric and arithmetic averages for ε and σ , respectively), and these are converted to transport properties and collision rates via isotropic 12/6 Lennard–Jones formulas.

In addition to errors associated with the use of simple combining rules, the 12/6 Lennard–Jones model ignores anisotropy in the intermolecular PES, the internal coordinates of the colliders, and the softness of the repulsive wall. While these errors can be important [21], particularly the error associated with the treatment of the repulsive wall [16,36], incorporating more detailed transport models into existing kinetics codes and databases remains rare. We therefore limit

attention to the prediction of the collision parameters ε and σ , despite the simplifications they represent.

We computed the collision parameters σ and ε using the “one-dimensional minimizations” method [67] and the distributed code 1DMIN [68]. In this approach, the inner turning point at the energy of the asymptote and the minimum energy of the interaction potential at several fixed orientations are averaged to determine σ and ε , respectively. Aside from special cases like A = H and H₂, which are not considered here, the use of these effective isotropic 12/6 Lennard–Jones parameters is not likely a significant source of error for transport and collision rate calculations in combustion, as previously quantified via comparisons with “exact” classical trajectory results [21] and with tabulated values [67].

The collision efficiency range parameter α . Detailed models for the collisional energy transfer function [22,38] have been shown to enable a priori kinetics predictions with errors of just 25% [22,69], whereas simpler models that incorporate fewer physical details, such as the “single-exponential-down” model [17,45] that is often used in energy-resolved master equation calculations [70–72], have a priori accuracies of closer to a factor of two [69,73–75]. Again, in an effort to be most directly useful for constructing extensive chemical kinetics tabulations, we restrict attention to models where collision outcomes are controlled by the single parameter $\alpha = \langle \Delta E_d \rangle$, which is the average energy transferred in deactivating collisions.

The computation of $\alpha = \langle \Delta E_d \rangle$ using our classical trajectory code DiNT [76] involves several steps, and our approach [22,55,67] is similar to approaches used by other groups [38–41,77]. Briefly, the unimolecular reactant A is prepared with a fixed class-dependent initial total energy E' representative of typical dissociation energies (here, 95 kcal/mol for alkanes, 90 kcal/mol for alcohols, and 45 kcal/mol for hydroperoxides) and an initial rotational state J' selected

from an independent thermal distribution at the temperature T of interest. As in Ref. [76], vibrationally averaged rotational constants, $\langle B \rangle$ and $\langle A \rangle$, are used to define the thermal populations from which J' is selected. For long linear systems (e.g., n -hexadecane), this choice results in significantly different computed values of α (by up to 50%) relative to the less accurate approach of using the equilibrium rotational constants, B_e and A_e . For systems with only a few heavy atoms $\langle B \rangle \approx B_e$, and the two approaches give similar results.

Some additional care must be taken when sampling the internal coordinates of the larger species, as well. We tested several strategies suitable for automation, and, with one exception, we found that our results were insensitive (within our sampling statistics) to the number of different initial low-energy conformers used to initiate the sampling trajectories (we tested using from 1 to 8 conformers) and to the length of the sampling trajectories (which we varied from 25 to 250 ps). The one exception we found is what might be considered the simplest approach. When we used only the linear geometry as the initial structure for the sampling trajectories along with short sampling times, we obtained fairly small (<30%) but statistically significant differences in α relative to the more robust strategies.

The relative collision parameters and any internal coordinates of the bath gas are selected from thermal distributions using standard approaches for bimolecular collisions [78]. The trajectories are propagated classically until A and M are separated enough to unambiguously determine the final state (E, J) of A, from which a variety of energy transfer properties can be computed including $\alpha = \langle \Delta E_d \rangle$. As has been frequently discussed (for example [22,23,33,38,77]), trajectory calculations (and experiments) necessarily describe *per-time* energy transfer averages. One must choose a reference collision rate constant Z to convert this information to the *per-*

collision averages, like α , that are often of interest. Here we use Z computed using the Lennard–Jones parameters obtained above.

Once the outcomes of an appropriately prepared trajectory ensemble are computed, one can generate any number of different energy- and angular–momentum-transfer averages as required for parameterizing more detailed higher-accuracy models for energy transfer [22,69], but this is not pursued here. Instead we analyze trends in the single moment α computed for a large number of systems. For each A + M and temperature T , 14400 trajectories were computed, which for our choices of numerical parameters resulted in 2-sigma Monte Carlo statistical uncertainties in α of $\sim 5\%$.

Throughout this work we report trends in $Zn_1\alpha$ instead of α , where n_1 is the number density of the bath gas at 1 Torr and the temperature of interest. The product $Z\alpha$ describes energy transferred per time and, neglecting angular momentum, is equal to the “deactivating” moment of the collisional energy transfer rate constant that is sometimes written $R(E,E')$, as discussed elsewhere [18,27]. We choose to multiply $Z\alpha$ by n_1 to give somewhat more manageable units (here, cm^{-1}/s). This choice of pressure is of no consequence as choosing pressures other than 1 Torr would simply scale all of the results equally. Trends in $Zn_1\alpha$ are often similar to trends in the per-collision quantity α , but the former avoids the arbitrariness associated with the particular choice of Z .

Data set. A total of 307 unimolecular reactants A with as many as sixteen heavy (nonhydrogen) atoms N were considered, including 141 hydrocarbons, 84 alcohols, and 82 hydroperoxides. Results are reported for several series of related systems where N is varied for a fixed branching and oxygen-group functionalization motif. These series are summarized in Tables 1 and 2, which include chemical drawings, and are described next.

The hydrocarbon systems studied here are shown in Table 1. In addition to the series of normal alkanes from methane to hexadecane ($N = 1-16$), we considered eight series of singly branched methyl- and ethyl- substituted alkanes (e.g., the series of 3-ethylalkanes from 3-ethylpentane, $N = 7$, to 3-ethyltetradecane, $N = 16$) and eight series of doubly branched dimethyl-substituted alkanes (e.g., the series of 2,2-dimethylalkanes from neopentane, $N = 5$, to 2,2-dimethyltetradecane, $N = 16$). Four series of highly branched species were considered: a “half methylated” series where every other C atom in the backbone was methyl-substituted, a “methylated” series where every C atom in the backbone was methyl-substituted, a “dimethylated” series where every C atom in the backbone was dimethyl-substituted, and a series representing the “iso” fuels isooctane, isododecane, and isohexadecane. We considered three series with alkane rings, including cyclopentane and cyclohexane with alkane chain substitutions of various lengths as well as a “polycyclo-” series consisting of cyclohexane, decalin, and the three-ring continuation of the series. Finally, we also considered the aromatic ring versions of the alkane ring series, where we note that the cyclopentadienyl- series consists of radicals, unlike all of the other systems considered here.

The oxygenated systems studied here are summarized in Table 2. In addition to the normal alcohol and hydroperoxide series, we considered several series of linear and branched alkanes substituted with one or two hydroxy or peroxy groups, as detailed in Table 2.

Automation. Collisional energy transfer parameters for all 307 systems in Tables 1 and 2 were computed at 1000 K and for $M = \text{Ar}$. Additional calculations at $T = 300$ and 2000 K and for $M = \text{He}, \text{H}_2,$ and N_2 were carried out for a subset of these systems. In total, 788 $A + M$ and T combinations were considered, requiring a total of more than 11 million trajectories. Managing such a large number of computations was aided by the following strategy.

The computation of σ , ε , and α was automated using three levels of codes and scripting:

(1) Chemical physics codes: At the lowest level, the chemical physics codes 1DMIN and DiNT read text input files and produce text output files, with the goal of keeping each step at this level as elementary as possible. 1DMIN is inherently simple, for example, requiring only the geometry of A, the identity of M, and the specification of the interaction potential as inputs. The output of 1DMIN is σ and ε . DiNT, on the other hand, has multiple uses, including geometry optimization, initial condition sampling, and trajectory simulations. These steps were carried out independently via separate instances of DiNT, with each step communicating via text inputs and producing different text outputs, as managed at the next level.

(2) Scripting: The following sequence of elementary chemical physics steps required to generate σ , ε , and α for a single system A + M and temperature T was scripted at the second level. The procedure started with a guessed geometry for A, the identity of the bath gas M, a potential energy surface for A + M, and the temperature T . (a) DiNT first optimized the structure of A. (b) 1DMIN read the optimized structure and computed σ and ε . (c) Independently, DiNT read the optimized structure and used it to launch a small number of long-lived trajectories of the isolated molecule A (i.e., without M present) designed to sample the internal coordinates and momenta of A microcanonically and subject to class-specific values of the initial energy E' . (d) Vibrationally-averaged rotational constants $\langle B \rangle$ and $\langle A \rangle$ were computed from the geometries generated in step c. (e) The results from steps a, c, and d were read and used by DiNT to set up and run an A + M collisional energy transfer ensemble. (f) The average energy transferred in deactivating collisions for the ensemble in step e was computed and renormalized to the collision rate Z generated from σ and ε computed in step b to produce α .

This stepwise scripting approach has the following useful features. First, intermediate information can be reused; for example, the internal coordinates for A sampled in step c can be reused for other bath gases. Second, the script can be readily restarted and naturally avoids repeating calculations while avoiding complex bookkeeping of the status of the various steps. Instead, each step has a set of input and output files associated with it. The script checks to see if the output file already exists, and, if so, the step is skipped. If the output file does not exist, the script checks for the required input files (which themselves may be output files from other steps). If the required input files do exist, the job is launched. If not, the step is skipped, presumably because steps involved in generating these files are still running or are yet to be run. The script can be rerun until all input and output files are produced and all steps are completed. Jobs managed in this way are easily parallelized despite the complex and heterogenous workflow, particularly when a computational cluster with a queuing system is used.

(3) Batch processing: At the highest level, simple and trivially parallelized batch scripts were used to loop through desired values of A, M, and T. At this level, one can also implement rules for specifying numerical parameters needed for the calculations, such as the maximum impact parameter, b_{\max} , or the center of mass distance used to terminate the trajectory, R_f , which may be system dependent. Here, for example, we generously set $b_{\max} = 8 + N/2 \text{ \AA}$ and $R_f = b_{\max} + 3 \text{ \AA}$. Such rules avoid the need for human intervention for each choice of A and allow for the rapid consideration of large numbers of systems. These scripts also collect and tabulate the desired information.

Trends. The major goal of the present work is to provide simple rules for estimating the collision parameters σ , ε , and α by studying their dependence on N and the structure of A. These rules are described next. As noted previously [55] and as demonstrated again in Sec. 3, the

Lennard–Jones parameters σ and ε are fairly insensitive to branching and may be well represented for each class of reactants and bath gas as a power law in the number of nonhydrogen (“heavy”) atoms N . Power law coefficients and exponents are newly determined here for alcohols and hydroperoxides, and we update our earlier determinations for hydrocarbons [55] to perform better for large N .

To estimate α , we define an effective number of heavy atoms N_{eff} that is based on the number and type of internal rotors in A. (We are using “rotor” here to mean any bonded pair of heavy atoms, including torsions as well as the constrained rotors appearing in rings.) If both central atoms are C atoms, we label the rotor based on the coordination (p, s, t, and q for primary, secondary, tertiary, or quaternary) of the two central C atoms. For example, propane has two ps rotors, and butane has two ps rotors and one ss rotor. Rotors where one or both of the central atoms is an O atom are counted separately as N_{CO} or N_{OO} . These counts are used to define N_{eff} via

$$\begin{aligned}
 N_{\text{eff}} = 1 &+ c_{\text{pp|ps|ss}} (N_{\text{pp}} + N_{\text{ps}} + N_{\text{ss}}) \\
 &+ c_{\text{pt|st}} (N_{\text{pt}} + N_{\text{st}}) \\
 &+ c_{\text{pq|sq}} (N_{\text{pq}} + N_{\text{sq}}) \\
 &+ c_{\text{tt|tq|qq}} (N_{\text{tt}} + N_{\text{tq}} + N_{\text{qq}}) \\
 &+ c_{\text{CO|OO}} (N_{\text{CO}} + N_{\text{OO}}) \\
 &+ c_{\text{ss,ring}} N_{\text{ss,ring}} - N_{\text{rings}} ,
 \end{aligned} \tag{1}$$

where the coefficients c_x scale contributions from the different rotor types, and we have grouped similar rotors together. We distinguish ss rotors appearing in rings from those that do not, and N_{rings} counts rings. When $c_x = 1$ for all x , N_{eff} is equal to the number of heavy atoms N . By choosing $c_x < 1$ for some terms, we show below that N_{eff} maps the computed values of α for branched and oxygenated species onto those for the corresponding normal (linear) series.

The coefficients in Eq. (1) may be systematically determined by considering subsets of systems that isolate the dependence of α on certain rotor types. This procedure will be described in Sec. 3, where we find $c_{\text{pp|ps|ss}} = 1$, $c_{\text{pt|st}} = \frac{2}{3}$, $c_{\text{pq|sq}} = \frac{1}{3}$, $c_{\text{tt|tq|qq}} = 0$, $c_{\text{CO|OO}} = \frac{1}{3}$, and $c_{\text{ss,ring}} = \frac{1}{2}$. Using

these parameters, α may be estimated for an unknown system as follows, so long as results for the corresponding normal (linear) series of α are known. We label the linear reference series $\bar{\alpha}$. One first counts rotor types and evaluates N_{eff} via Eq. (1), which may be a non-integer number. One may be tempted to estimate α as $\bar{\alpha}(N_{\text{eff}})$ by interpolating nearby values of $\bar{\alpha}$, which of course is known only at integer values of N . Such a procedure would not properly account for changes in the collision rate with N , however. Instead, one should interpolate the product $\overline{Z\alpha}$ for the reference series to determine its value at N_{eff} and then divide by Z for the system size of interest N , i.e.,

$$\alpha \approx \overline{Z\alpha}(N_{\text{eff}})/Z(N). \quad (2)$$

An example of this procedure is given at the end of Sec. 3, and a spreadsheet useful for evaluating Eq. (2) is given as supporting information. The supporting information also includes results for every system studied here, including all of the useful data appearing in the figures as well as results for temperatures and bath gases mentioned but not presented.

3. RESULTS AND DISCUSSION

Collision rate constants. Lennard–Jones parameters σ and ε were computed for the large set of A + M systems discussed above. Figure 1 shows the results of these calculations for M = Ar converted to Lennard-Jones collision rate constants Z at 1000 K. For a given value of N , the scatter in Z is small enough (typically less than 5%) to neglect for many applications. We therefore express σ and ε as simple functions of N . The results from Fig. 1 for M = Ar are well represented by the expressions

hydrocarbons (+Ar)	$\sigma(N) = 3.40 N^{0.18} \text{ \AA}$	$\varepsilon(N) = 113 N^{0.31} \text{ cm}^{-1}$
alcohols (+Ar)	$\sigma(N) = 3.05 N^{0.20} \text{ \AA}$	$\varepsilon(N) = 150 N^{0.29} \text{ cm}^{-1}$
hydroperoxides (+Ar)	$\sigma(N) = 3.05 N^{0.20} \text{ \AA}$	$\varepsilon(N) = 110 N^{0.39} \text{ cm}^{-1}$

where we have improved our previous recommendation for hydrocarbons [55] to better represent $N > 8$. The lines in Fig. 1 show the values of Z computed using these expressions. This procedure was repeated for $M = \text{He}, \text{H}_2,$ and N_2 , and we obtained

hydrocarbons (+He)	$\sigma(N) = 3.33 N^{0.17} \text{ \AA}$	$\varepsilon(N) = 21.3 N^{0.31} \text{ cm}^{-1}$
hydrocarbons (+H ₂)	$\sigma(N) = 3.15 N^{0.18} \text{ \AA}$	$\varepsilon(N) = 75.0 N^{0.30} \text{ cm}^{-1}$
hydrocarbons (+N ₂)	$\sigma(N) = 3.68 N^{0.16} \text{ \AA}$	$\varepsilon(N) = 100. N^{0.25} \text{ cm}^{-1}$
alcohols (+He)	$\sigma(N) = 2.90 N^{0.21} \text{ \AA}$	$\varepsilon(N) = 22.0 N^{0.28} \text{ cm}^{-1}$
hydroperoxides (+He)	$\sigma(N) = 2.90 N^{0.21} \text{ \AA}$	$\varepsilon(N) = 10.0 N^{0.75} \text{ cm}^{-1}$

Tests of the intramolecular potential. Next we briefly consider the sensitivity of the computed values of α to the description of the intramolecular potential. The collision rate constants Z are independent of this choice. Figure 2 shows $Zn_1\alpha$ computed for the series of n -alkanes in Ar at 1000 K using three molecular mechanics potentials (MM3, AMOEBA09, and OPLSAA) and one semiempirical tight binding (TB) potential. These results are seen to increase nearly linearly with N for small N , they begin to plateau around pentane, and are relatively independent of N for large N . The value of N at which this transition takes place is related to the system size at which the bath gas temperature equals the effective temperature of the internal energy of A.

Results for the three molecular mechanics potentials agree with each other within their 5% 2-sigma statistical sampling uncertainties, whereas results for the TB potential are slightly but systematically lower (by 10%) for alkanes larger than hexane. The TB potential has an unphysical description of torsions, which likely explains this result. The relative insensitivity of collisional energy transfer efficiencies on the description of the intramolecular potential has been noted previously [28,30] and is confirmed again here in this somewhat different context. The MM3 parameterization is used exclusively in the remainder of this work.

Lightly branched alkanes. Figure 3 shows $Zn_1\alpha$ at 1000 K for the alkane series listed in Table 1. In Fig. 3a, results for the n -alkanes are compared with those for the series of singly and

doubly branched alkanes as a function of N . As in Fig. 2, the 2-sigma statistical uncertainties for these results are $\sim 5\%$, and so we do not attempt to interpret the fine structure of any of these curves. Instead, we note qualitatively that the curves for the singly branched species appear shifted to the right by ~ 1 heavy atom relative to the n -alkanes, whereas the curves for the doubly branched species appear shifted by ~ 2 heavy atoms. These qualitative observations were made previously [55] and were the initial motivation for the design of Eq. (1).

The parameters in Eq. (1) were systematically determined by considering subsets of these data that isolated different rotor types, as marked in Table 1. We first considered the singly branched methyl- and ethyl- series, which feature pt and st rotor types in addition to ps and ss rotor types found in the n -alkane series. By setting $c_{pp|ps|ss} = 1$ and optimizing the single remaining parameter required to describe these series, $c_{pt|st} = \frac{2}{3}$, we found that the resulting values of N_{eff} closely mapped the K -methylalkane and K -ethylalkane results onto the n -alkane series. Similarly, by considering the 2,3-dimethylalkane series, which features tt rotors, and the K,K -dimethylalkane series, which features pq and sq rotors, we determined $c_{tt|tq|qq} = 0$ and $c_{pq|sq} = \frac{1}{3}$, respectively. Figure 3c shows the results of these three optimizations, where it can be clearly seen that N_{eff} regularizes the results of all 16 branched series (83 systems) to closely match the n -alkane series.

The relationship between N and N_{eff} may be clarified using neopentane as an example, which is the first entry in the 2,2-dimethylalkane series. Its computed collision parameters at 1000 K and for $M = \text{Ar}$ are $\alpha = 501 \text{ cm}^{-1}$ and $Z = 5.65 \times 10^{-10} \text{ cm}^3 \text{ molecule}^{-1} \text{ s}^{-1}$, corresponding to $Zn_1\alpha = 2.73 \times 10^9 \text{ cm}^{-1}/\text{s}$ at 1 Torr Ar, as shown in Fig. 3. For this system, $N = 5$, and n -pentane at these same conditions has a similar collision rate ($Z = 5.77 \times 10^{-10} \text{ cm}^3 \text{ molecule}^{-1} \text{ s}^{-1}$) but a much ($\sim 60\%$) larger value of $\alpha = 786 \text{ cm}^{-1}$. According to Eq. (1), however, neopentane's four pq rotors give N_{eff}

$= 2\frac{1}{3}$, suggesting instead that neopentane should have energy transfer properties more similar to ethane ($\alpha = 473 \text{ cm}^{-1}$) and propane ($\alpha = 612 \text{ cm}^{-1}$) than *n*-pentane, which is in fact the case.

Physically, it appears reasonable to interpret $c_{\text{pp|ps|ss}} = 1$ and our empirically optimized values of $c_{\text{pt|st}} = \frac{2}{3}$, $c_{\text{pq|sq}} = \frac{1}{3}$, and $c_{\text{tt|tq|qq}} = 0$ as follows. Rotors involving *only* primary and secondary carbons (as in the pp|ps|ss group) are sufficiently unhindered so as to each contribute equally to energy transfer ($c_{\text{pp|ps|ss}} = 1$), on average. Increasing coordination of the C atoms participating in the rotors leads to more hindrance and evidently less efficient promotion of energy transfer, again, on average. Partially hindered rotors involving just one tertiary carbon atom or just one quaternary carbon atom (as in the pt|st and pq|sq groups) are less efficient but remain active ($c_{\text{pt|st}} = \frac{2}{3}$ and $c_{\text{pq|sq}} = \frac{1}{3}$), whereas more strongly hindered rotors that involve two tertiary and/or quaternary carbon atoms are not active ($c_{\text{tt|tq|qq}} = 0$).

Heavily branched alkanes. In Figs. 3b and 3d, we test the above determinations of $c_{\text{pp|ps|ss}}$, $c_{\text{pt|st}}$, and $c_{\text{pq|sq}}$ for several highly branched alkanes. As seen in Fig. 3b, there is considerable variation in this set of results, which includes strongly hindered species like those in the “dimethylated” and “‘iso’ fuels” series defined in Table 1. Nonetheless, the three coefficients determined above for the singly and doubly branched species continue to work well for heavily branched species, as shown in Fig. 3d. This result supports the assumption that the rotor corrections are additive, as in Eq. (1).

In both Figs. 3c and 3d, the dispersion in the results increases for large N_{eff} , suggesting additional errors in the N_{eff} approach for larger systems. The worst performance of Eq. (1) in Fig. 3d is for the “half methylated” series, where the use of N_{eff} offers little improvement over simply using N to characterize its energy transfer for the largest members of the series. These additional errors may indicate the need for more complicated rules, such as nonadditive rotor (i.e., multirotor)

corrections and/or finer classifications of rotor types. These strategies were not pursued here, and we simply note that the maximum deviation in the results for large N_{eff} is 20%. We do include a special treatment for rings, however, as discussed next.

Rings. Results for three series of species with alkane rings, as described in Table 1, are also shown in Figs. 3b and 3d. For these systems, the performance of the coefficients determined above was found to be poor enough that we pursued a special correction for rotors appearing in rings. Such a correction may again be physically motivated by considering the hinderance of the rotors involved, as one expects, e.g., ss rotors appearing in rings to be more hindered than ss rotors appearing in linear chains. Empirically, we find that setting $c_{\text{ss,ring}} = \frac{1}{2}$ gives values of N_{eff} that are good predictors of collisional energy transfer, as shown in Fig. 3d. Note that rings have one “extra” torsion relative to linear alkanes of the same size, which leads to the $-N_{\text{rings}}$ term in Eq. (1) and thus complicates the interpretation of $c_{\text{ss,ring}} = \frac{1}{2}$. Still, it is notable that our empirical optimizations indicate that ss rotors appearing in rings are intermediate in their efficiency in promoting energy transfer relative to the pt|st and pq|sq groups.

Cyclic aromatic alkenes. The above tests could be repeated for analogous series of unsaturated systems and radicals, but we do not present such tests here. Instead, we briefly consider three series with aromatic hydrocarbon rings, again as summarized in Table 1, due to the importance of their energy transfer properties controlling molecular growth pathways [79,80]. As shown in Fig. 3d, the coefficients optimized for alkanes continue to work well for unsaturated rings, with no special corrections for PAHs, e.g., evidently needed.

Alcohols and hydroperoxides. Next we consider the 13 series of alcohols and 13 series of hydroperoxides described in Table 2. These series include singly and doubly branched species and some series with two oxygen-containing functional groups (e.g., diols). Figures 4a and 4b show

the computed values of $Zn_1\alpha$ at 1000 K and 1 Torr Ar for the alcohol and hydroperoxide series, respectively. Relative to the alkane series, the oxygenated systems have lower values of $Zn_1\alpha$ that “plateau” at smaller N , with this behavior appearing more prominently for the hydroperoxides than the alcohols. These trends are consistent with the lower initial internal energies for these groups (90 and 45 kcal/mol for the alcohols and hydroperoxides, respectively) relative the alkanes (95 kcal/mol).

With the alkane coefficients in Eq. (1) fixed at the values determined above, we optimized the single remaining parameter $c_{CO|OO} = \frac{1}{3}$ so as to best map the results of the branched and multifunctional oxygenated species onto their respective normal series via N_{eff} . The results of this optimization are shown in Figs. 4c and 4d, where the usefulness of using N_{eff} instead of N to predict collisional energy transfer is again clearly demonstrated. The worst performance of the N_{eff} approach in Fig. 4 is for the series of diperoxyalkanes, but we note that the maximum dispersion of the results in Fig. 4d is still less than 15%.

Transferability to other temperatures and other bath gases. A subset of the systems in Figs. 3 and 4 were studied at 300 and 2000 K, again for $M = \text{Ar}$. Results at 2000 K are very similar to those for 1000 K in Figs. 3 and 4 and are not shown. Figure 5 shows the results of these tests at 300 K for thirteen series, where the N_{eff} model is again found to work well. We emphasize that the coefficients in Eq. (1) optimized using the 1000 K data were not reoptimized when constructing Figs. 5c and 5d. The good performance of N_{eff} in Figs. 5c and 5d at 300 K and at 2000 K demonstrates that the coefficients in Eq. (1) are indeed transferable to other temperatures, which greatly increases the utility of the approach.

Transferability was tested for the baths $M = \text{He}, \text{H}_2$ and N_2 , and Fig. 6 shows a subset of these tests for alkanes + He and N_2 . Results for alcohols and hydroperoxides + He and for alkanes

+ H₂ are qualitatively similar to those for the alkanes + He and are not shown. The parameterizations determined above for M = Ar are shown to work very well for M = N₂ (Fig. 6d) but they are somewhat less accurate for M = He (Fig. 6a). It may be of interest to develop bath-specific coefficients for Eq. (1), but we do not pursue this here.

Estimating the collision parameters σ , ε , and α . In this section we summarize the use of N and N_{eff} to estimate collision parameters. One can trivially compute σ and ε for hydrocarbons, alcohols, and hydroperoxides by simply counting the number of nonhydrogen atoms N and using the formulas given at the beginning of this section. We did not consider M = H₂ or N₂ for alcohols and hydroperoxides, but it is likely a good approximation to use assume their values of σ and ε are close to those for M = He or Ar, respectfully, if no better information is available. Similarly, values for M = Ar (or M = N₂, if available) are likely suitable for describing M = Kr, O₂, and CO with sufficient accuracy for many applications. Note also that the collision rates Z for alcohols and hydroperoxides are very similar to one another for a given value of N , and so, again in the absence of better information, it appears reasonable to apply these same formulas to other oxygenated classes of species. Finally, we note that when more accurate values of σ and ε are deemed necessary, one can compute them directly fairly readily using the “one-dimensional minimizations” approach [67] so long as not too many are needed. Higher-accuracy calculations of transport properties are also possible, although these typically require somewhat more computational effort [16,21].

The direct computation of α requires a nontrivial amount of effort, and a major result from the present work is the strategy for using N_{eff} to avoid this effort. As a demonstration, we consider 2,2,3-trimethylbutane (TMB) + Ar at 1000 K, which was not included in any of the series in Table 1. TMB ($N = 7$) has one tq rotor, two pt rotors, and three pq rotors, such that Eq. (1) evaluates to

$N_{\text{eff}} = 3\frac{1}{3}$. This value of N_{eff} indicates that TMB's collision properties should be intermediate of propane's ($\bar{\alpha}(3) = 612 \text{ cm}^{-1}$) and butane's ($\bar{\alpha}(4) = 704 \text{ cm}^{-1}$). Simply interpolating these values gives 643 cm^{-1} , but as noted in Sec. 2 such a procedure does not properly account for changes in the collision rate with N . Instead, we evaluate Eq. (2) for $N_{\text{eff}} = 3\frac{1}{3}$ and $N = 7$ as follows.

For the denominator of Eq. (2), $Z(N = 7)$, we could either simply adopt *n*-heptane's Lennard–Jones parameters ($\sigma = 4.80 \text{ \AA}$ and $\varepsilon = 205 \text{ cm}^{-1}$) and compute Z or else evaluate the expressions given at the beginning of this section ($\sigma = 4.83 \text{ \AA}$ and $\varepsilon = 215 \text{ cm}^{-1}$). These two approaches result in collision rate constants Z that differ by just a few percent. To evaluate the numerator of Eq. (2), we need to interpolate the product $\overline{Z\alpha}$ for $N_{\text{eff}} = 3\frac{1}{3}$. From trajectory calculations, we know that $\overline{Z\alpha}(3) = 315$ and $\overline{Z\alpha}(4) = 383$ for propane and butane + Ar at 1000 K, respectively (in both cases the unwieldy units are $10^9 \text{ cm}^3 \text{ molecule}^{-1} \text{ s}^{-1} \text{ cm}^{-1}$). Linearly interpolating these numbers gives $\overline{Z\alpha}(N_{\text{eff}} = 3\frac{1}{3}) = 338$, which, when divided by 10^9 and the collision rate constant $Z(7) = 6.38 \times 10^{-10} \text{ cm}^3 \text{ molecule}^{-1} \text{ s}^{-1}$, gives $\alpha \approx 529 \text{ cm}^{-1}$.

The estimates obtained via this procedure ($\sigma = 4.83 \text{ \AA}$, $\varepsilon = 215 \text{ cm}^{-1}$, and $\alpha = 529 \text{ cm}^{-1}$) are in very good agreement ($< 6\%$) with the results of a direct calculations for this system ($\sigma = 4.75 \text{ \AA}$, $\varepsilon = 206 \text{ cm}^{-1}$, and $\alpha = 560 \pm 28 \text{ cm}^{-1}$). If we had instead adopted heptane's value of α for TMB, $\bar{\alpha}(7) = 797 \text{ cm}^{-1}$, our estimate of α would have had an error of $\sim 40\%$.

The use of N_{eff} to estimate α relies on knowing $\overline{Z\alpha}$ for the corresponding normal (linear) series and for the bath gas and temperature of interest. The results calculated here for the normal alkane series + He, Ar, H₂, and N₂ and for the normal alcohol and hydroperoxides series + He and Ar are given as supporting information, along with analytic formulas fit to these data to aid in the evaluation of Eq. (2) for non-integer N_{eff} . If no better information is available, it is likely a good

approximation to use the values of α estimated from these series for $M = \text{Ar}$ or N_2 to describe $M = \text{Kr}, \text{N}_2, \text{O}_2,$ and CO , as these species often have similar energy transfer parameters.

4. CONCLUSIONS

The computation of Lennard–Jones collision parameters σ and ε and the collision efficiency range parameter α was automated and carried out for 307 alkanes, alcohols, and hydroperoxides, the He, Ar, H_2 , and N_2 baths, and at 300, 1000, and 2000 K. This data set was analyzed to develop simple rules for predicting σ and ε based on the type of unimolecular reactant, the number of nonhydrogen atoms N , and the bath gas. For estimating α , we demonstrated the utility of determining an effective number of heavy atoms N_{eff} based on the numbers and types of internal rotors in the system.

The empirical hindering correction parameters that define N_{eff} via Eq. (1) were derived and tested using a large data set for $M = \text{Ar}$ at 1000 K. We demonstrated the excellent and good transferability of these parameters to other temperatures and bath gases, respectively. This transferability greatly increases the utility of the approach, which should be useful for the rapid estimation of transport parameters and collision efficiencies for large numbers of alcohols, hydroperoxides, and alkanes. This approach is likely readily extended without significant modification to the treatment of more classes of unimolecular reactants A, including unsaturated and radical species. The extension to more bath gases, including strong colliders such as $M = \text{H}_2\text{O}$ and CO_2 , may require further validation of the approach and perhaps specialized bath-specific parameterizations.

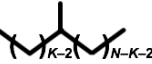
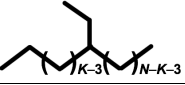
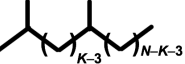
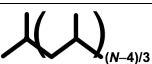
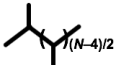
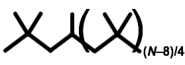
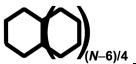
Physically, the “effective internal rotor” approach for determining N_{eff} , while empirical, can be readily motivated by speculating that more strongly hindered rotors, such as those involving

tertiary C atoms or appearing in rings, are less efficient at promoting collisional energy transfer, on average, than the relatively unhindered rotors appearing in normal alkanes, alcohols, and hydroperoxides. Closely related explanations based on the size and shape of A, its rotational constants, its vibrational frequencies and in particular its number of low frequency vibrations, etc. could also be inferred from these results. It may be of interest to interrogate the results of the trajectories in more detail to further explore these relationships and to provide a more definitive motivation for Eq. (1), but we have not done so here.

ACKNOWLEDGMENTS

This work was supported by the U. S. Department of Energy, Office of Basic Energy Sciences, Division of Chemical Sciences, Geosciences, and Biosciences, under Contract Number DE-AC02-06CH11357 and in part by the Argonne–Sandia Consortium on High-Pressure Combustion Chemistry (ANL FWP 59044). We gratefully acknowledge computing resources provided by Bebop, a high-performance computing cluster operated by the Laboratory Computing Resource Center at Argonne National Laboratory.

Table 1. Series of hydrocarbons

Series	Drawing	M^a	Series ^b	pp ps ss	pt st	tt tq qq	pq sq	ss,ring
<i>n</i> -alkanes		12	$N=1(1)8,10(2)16$	X				
<i>Singly branched</i>		39						
<i>K</i> -methyl-		25	$K=2(1)4,6,8;$ $N=2K(1)8,10(2)16$	X	X			
<i>K</i> -ethyl-		14	$K=3; N=7,8(2)16$ $K=4; N=9,10(2)16$ $K=6; N=13,14,16$	X	X			
<i>Doubly branched</i>		44						
2, <i>K</i> -dimethyl-		22	$K=3; N=6(1)8,10(2)16$ $K=4; N=7,8,10(2)16$ $K=6; N=9,10(2)16$ $K=8; N=11,12(2)16$	X	X	X		
<i>K,K</i> -dimethyl-		22	$K=2; N=5(1)8,10(2)16$ $K=3; N=7,8,10(2)16$ $K=4; N=9,10(2)16$ $K=6; N=13,14,16$	X			X	
<i>Highly branched</i>		16						
“half methylated”		4 ^c	$N=7(3)16$		X			
“methylated”		6 ^c	$N=6(2)16$		X	X		
“dimethylated”		3	$N=8(3)14$			X	X	
“‘iso’ fuels”		3	$N=8,12,16$		X		X	
<i>Alkane rings</i>		16						
cyclopentyl-		7	$N=6(1)8,10(2)16$	X	X			X
cyclohexyl-		6	$N=7,8(2)16$	X	X			X
polycyclo-		3	$N=6,10,14$	X	X			X
<i>Aromatic rings</i>		16						
cyclopenta-dienyl-		7	$N=6(1)8,10(2)16$	X	X			X
phenyl-		6	$N=7,8(2)16$	X	X			X
anthracenes		3	$N=6,10,14$	X	X			X

^a M is the number of species considered in each group. ^bThe notation $X(Y)Z$ indicates a list from X to Z in steps of Y . ^cThe first member in the series also appears in a dimethyl series.

Table 2. Series of alcohols and hydroperoxides

Series	Drawing	M^a	Series ^b	pp ps ss	pt st	tt tq qq	pq sq	CO O
<i>Alcohols</i>								
<i>n</i> -alcohols		11	$N=2(1)9,11(2)15$	X				X
<i>K</i> -ols		24	$K=2(1)4;$ $N=2K(1)9,11(2)15$ $K=6;N=12,13,15$	X	X			X
<i>K,K</i> -diols		23	$K=2(1)4;$ $N=2K+1(1)10,12(2)16$ $K=6;N=13,14,16$	X			X	X
<i>K</i> -methyl- <i>K</i> -ols		14	$K=2,3;$ $N=2K+1(1)9,11(2)15$	X	X	X	X	X
<i>K</i> -methyl- <i>L</i> -ols		12	$K=2;L=3;N=7(1)9,11(2)15$ $K=3;L=2;N=7(1)9,11(2)15$	X	X	X	X	X
<i>Hydroperoxides</i>								
<i>n</i> -hydroperoxides		10	$N=3(1)10,12,14$	X				X
<i>K</i> -peroxy-		23	$K=2;N=5(1)10,12(2)16$ $K=3;N=7(1)9,12(2)16$ $K=4;N=9,10(2)16$ $K=6;N=13,14,16$	X	X			X
<i>K,K</i> -diperoxy-		23	$K=2;N=7(1)14,16$ $K=3;N=9(1)14,16$ $K=4;N=11(1)14,16$ $K=6;N=15,16$	X			X	X
<i>K</i> -methyl- <i>K</i> -peroxy-		13	$K=2;N=6(1)10,12,14$ $K=3;N=8,9,10(2)14$	X	X	X	X	X
<i>K</i> -methyl- <i>L</i> -peroxy-		13	$K=2;L=3;N=7(1)9,10(2)16$ $K=3;L=2;N=8,9,10(2)16$	X	X	X	X	X

^a M is the number of species considered in each group. ^bThe notation $X(Y)Z$ indicates a list from X to Z in steps of Y .

REFERENCES

- ¹ Richter, H.; Granata, S.; Green, W. H.; Howard, J. B. *Proc. Combust. Inst.* 2005, 30, 1397–1405.
- ² Davis, S. G.; Joshi, A. V.; Wang, H.; Egolfopoulos, F. *Proc. Combust. Inst.* 2005, 30, 1283–1292.
- ³ Sivaramakrishnan, R.; Brezinsky, K.; Dayma, G.; Dagaut, P. *Phys. Chem. Chem. Phys.* 2007, 9, 4230–4244.
- ⁴ Dooley, S.; Won, S. H.; Chaos, M.; Heyne, J.; Ju, Y. G.; Dryer, F. L.; Kumar, K.; Sung, C. J.; Wang, H. W.; Oehlschlaeger, M. A.; Santoro, R. J.; Litzinger, T. A. *Combust. Flame* 2010, 157, 2333–2339.
- ⁵ Mehl, M.; Pitz, W. J.; Westbrook, C. K.; Curran, H. J. *Proc. Combust. Inst.* 2011, 33, 193–200.
- ⁶ Kéromnés, A.; Ketcalfé, W. K.; Heufer, K. A.; Donohoe, N.; Das, A. K.; Sung, C.-J.; Herzler, J.; Naumann, C.; Griebel, P.; Mathieu, O.; Krejci, M. C.; Peterson, E. L.; Pitz, W. J.; Curran, H. J. *Combust. Flame* 2013, 160, 995–1011.
- ⁷ Sarathy, S. M.; Oßwalt, P.; Hansen, N.; Kohse-Höinghaus, K. *Prog. Energy Combust. Sci.* 2014, 44, 40–102.
- ⁸ Curran, H. J. *Proc. Combust. Inst.* 2019, 37, 57–81.
- ⁹ Konnov, A. A. *Combust. Flame* 2019, 203, 14–22.
- ¹⁰ Miller, J. A.; Pilling, M. J.; Troe, J. J. *Proc. Combust. Inst.* 2005, 30, 43–88.
- ¹¹ Pilling, M. J. *Proc. Combust. Inst.* 2009, 32, 27–44.
- ¹² Vereecken, L.; Glowacki, D. R.; Pilling, M. J. *Chem. Rev.* 2015, 115, 4063–4114.
- ¹³ Klippenstein, S. J. *Proc. Combust. Inst.* 2017, 36, 77–111.

- ¹⁴ Mason, E. A. In *Kinetic Processes in Gases and Plasmas*, Hochstim, A. R., Ed.; Academic Press: London, 1969; pp. 57–97.
- ¹⁵ Brown, N. J.; Bastian, L. A. J.; Price, P. N. *Prog. Energy Combust. Sci.* 2011, 37, 565.
- ¹⁶ Dagdigian, P. J. *Combust. Flame* 2015, 162, 2480.
- ¹⁷ Troe, J. J. *Chem. Phys.* 1977, 66, 4745; *ibid.*, 4758.
- ¹⁸ Gilbert, R. G. *Int. Rev. Phys. Chem.* 1991, 10, 319–347.
- ¹⁹ Barker, J. R.; Golden, D. M. *Chem. Rev.* 2003, 103, 4577.
- ²⁰ Miller, J. A.; Klippenstein, S. J. *J. Phys. Chem. A* 2006, 110, 10528.
- ²¹ Jasper, A. W.; Kamarchik, E.; Miller, J. A.; Klippenstein, S. J. *J. Chem. Phys.* 2014, 141, 124313.
- ²² Jasper, A. W.; Pelzer, K. M.; Kamarchik, E.; Harding, L. B.; Klippenstein, S. J. *Science* 2014, 346, 1212.
- ²³ Brown, N. J.; Miller, J. A. *J. Chem. Phys.* 1984, 80, 5568–5580.
- ²⁴ Schranz, H. W.; Troe, J. J. *Phys. Chem.* 1986, 90, 6168–6175.
- ²⁵ Hu, X.; Hase, W. L. *J. Phys. Chem.* 1988, 92, 4040–4064.
- ²⁶ Lendvay, G.; Schatz, G. C. *J. Phys. Chem.* 1990, 94, 8864–8866.
- ²⁷ Lim, K. F.; Gilbert, R. G. *J. Phys. Chem.* 1990, 94, 72–77.
- ²⁸ Lendvay, G.; Schatz, G. C. *J. Phys. Chem.* 1992, 96, 3752–3756.
- ²⁹ Lenzer, T.; Luther, K.; Troe, J.; Gilbert, R. G.; Lim, K. F. *J. Chem. Phys.* 1995, 103, 626.
- ³⁰ Merouch, O.; Hase, W. L. *J. Phys. Chem. A* 1999, 103, 3981.
- ³¹ Barker, J. R.; Yoder, L. M.; King, K. D. *J. Phys. Chem. A* 2001, 105, 796–809.
- ³² Bernshtein, V.; Oref, I. *Isr. J. Chem.* 2007, 47, 205.

- ³³ Lendvay, G. In *Unimolecular Kinetics: Parts 2 and 3: Collisional Energy Transfer and the Master Equation*, Robertson, S. H., Ed.; Elsevier: 2019; Vol. 43, pp. 110–272.
- ³⁴ Hutson, J. M.; McCourt, F. R. *J. Chem. Phys.* 1983, 80, 1135.
- ³⁵ Stallcop, J. R.; Partridge, H.; Walch, S. P.; Levin, E. J. *J. Chem. Phys.* 1992, 97, 3431.
- ³⁶ Middha, P.; Yang, B.; Wang, H. *Proc. Combust. Inst.* 2002, 29, 1361.
- ³⁷ Dagdigian, P. J.; Klos, J.; Warehime, M.; Alexander, M. H. *J. Chem. Phys.* 2016, 145, 164309.
- ³⁸ Barker, J. R.; Weston, R. E. *J. Phys. Chem. A* 2010, 114, 10619–10633; 2012, 116, 799(E).
- ³⁹ Conte, R.; Houston, P. L.; Bowman, J. M. *J. Phys. Chem. A* 2014, 118, 7742.
- ⁴⁰ Matsugi, A. *J. Phys. Chem. A* 2018, 8, 1972–1985.
- ⁴¹ Wang, J.; Wen, K.; You, X.; Mao, Q.; Luo, K. H.; Pilling, M. H.; Robertson, S. H. *J. Chem. Phys.* 2019, 151, 044301.
- ⁴² Ahumada, J. J.; Michael, J. V.; Osborne, D. T. *J. Chem. Phys.* 1972, 57, 3736–3745.
- ⁴³ Michael, J. V.; Osborne, D. T.; Suess, G. N. *J. Chem. Phys.* 1973, 58, 2800.
- ⁴⁴ Michael, J. V.; Payne, W. A.; Whytock, D. A. *J. Chem. Phys.* 1976, 65, 4830–4834.
- ⁴⁵ Tardy, D. C.; Rabinovich, B. S. *Chem. Rev.* 1977, 77, 369–408.
- ⁴⁶ Barnes, R. W.; Pratt, G. L.; Wood, S. W. *J. Chem. Soc. Faraday Trans.* 1989, 85, 229–238.
- ⁴⁷ Yerram, M. L.; Brenner, J. D.; King, K. D.; Barker, J. R. *J. Phys. Chem.* 1990, 94, 6341–6350.
- ⁴⁸ Feng, Y.; Niiranen, J. T.; Bencsura, A.; Knyazev, V. D.; Gutman, D. *J. Phys. Chem.* 1993, 97, 871–880.
- ⁴⁹ Fletcher, F. J.; Rabinovitch, B. S.; Watkins, K. W.; Locker, D. J. *J. Phys. Chem.* 1996, 70, 2823–2833.

- ⁵⁰ Michael, J. V.; Su, M.-C.; Sutherland, J. W.; Carroll, J. J.; Wagner, A. F. J. *Phys. Chem. A* 2002, 106, 5297–5313.
- ⁵¹ Altinay, G.; Macdonald, R. G. *J. Phys. Chem. A* 2012, 116, 1353–1367.
- ⁵² Altinay, G.; Macdonald, R. G. *J. Phys. Chem. A* 2012, 116, 2161–2176.
- ⁵³ Shao, J.; Choudhary, R.; Susa, A.; Davidson, D. F.; Hanson, R. K. *Proc. Combust. Inst.* 2019, 37, 145–152.
- ⁵⁴ Choudhary, R.; Girard, J. J.; Shao, J.; Davidson, D. F.; Hanson, R. K. *Combust. Flame* 2019, 203, 265–278.
- ⁵⁵ Jasper, A. W.; Oana, C. M.; Miller, J. A. *Proc. Combust. Inst.* 2015, 35, 197–204.
- ⁵⁶ Jasper, A. W.; Davis, M. J. *J. Phys. Chem. A* 2019, 123, 3464–3480.
- ⁵⁷ Jasper, A. W.; Miller, J. A. *J. Phys. Chem. A* 2011, 115, 6438–6455.
- ⁵⁸ Stace, A. J.; Murrell, J. N. *J. Chem. Phys.* 1978, 68, 3028–3039.
- ⁵⁹ Gallucci, C. R.; Schatz, G. C. *J. Phys. Chem.* 1982, 86, 2352–2358.
- ⁶⁰ Yan, T.; Hase, W. L. *J. Phys. Chem. B* 2002, 106, 8029–8037.
- ⁶¹ Majumder, M.; Gibson, K. D.; Sibener, S. J.; Hase, W. L. *J. Phys. Chem. C* 2018, 122, 16048–16059.
- ⁶² Ponder, J. W.; TINKER – Software Tools for Molecular Design, Version 6: Washington University Medical School, 2011.
- ⁶³ Allinger, N. L.; Yuh, Y. H.; Lii, J. H. *J. Am. Chem. Soc.* 1989, 111, 8551–8566.
- ⁶⁴ Cornell, W. D.; Cieplak, P.; Bayly, C. I.; Gould, I. R.; Merz, K. M.; Ferguson, D. M.; Spellmeyer, D. C.; Fox, T.; Caldwell, J. W.; Kollman, P. A. *J. Am. Chem. Soc.* 1995, 117, 5179–5197.

- ⁶⁵ Jorgensen, W. L.; Maxwell, D. S.; Tirado-Rives, J. J. *Am. Chem. Soc.* 1996, 118, 11225–11236.
- ⁶⁶ Wang, Y.; Mak, C. H. *Chem. Phys. Lett.* 1995, 235, 37–46.
- ⁶⁷ Jasper, A. W.; Miller, J. A. *Combust. Flame* 2014, 161, 101–110.
- ⁶⁸ Jasper A. W.; Miller, J. A. OneDMin: A code for calculating Lennard-Jones parameters from detailed intermolecular potentials via one-dimensional minimizations, July 2014. (available online at <https://tcg.cse.anl.gov/papr/codes/onedmin.html>)
- ⁶⁹ Jasper, A. W. *J. Phys. Chem. A* 2020, 124, 1205–1226.
- ⁷⁰ Barker, J. R.; Golden, D. M. *Chem. Rev.* 2003, 103, 4577–4591.
- ⁷¹ Pilling, M. J.; Robertson, S. H. *Annu. Rev. Phys. Chem.* 2003, 54, 245–275.
- ⁷² Miller, J. A.; Klippenstein, S. J. *J. Phys. Chem. A* 2006, 110, 10528–10544.
- ⁷³ Jasper, A. W.; Miller, J. A.; Klippenstein, S. J. *J. Phys. Chem. A* 2013, 117, 12243–12255.
- ⁷⁴ Tranter, R. S.; Jasper, A. W.; Randazzo, J. B.; Lockhart, J. P. A.; Porterfield, J. P. *Proc. Combust. Inst.* 2017, 36, 211–218.
- ⁷⁵ Jasper, A. W.; Miller, J. A. *J. Phys. Chem. A* 2009, 113, 5612–5619.
- ⁷⁶ Jasper, A. W.; Oana, C. M.; Truhlar, D. G. DiNT: Direct Nonadiabatic Trajectories, July 2013. (available online at <https://tcg.cse.anl.gov/papr/codes/dint.html>)
- ⁷⁷ Lim, K. F.; Gilbert, R. G. *J. Phys. Chem.* 1990, 94, 72–77.
- ⁷⁸ Truhlar, D. G.; Muckerman, J. T. In *Atom-Molecule Collision Theory: A Guide for the Experimentalist*; Bernstein, R. B. Ed.; Plenum Press: New York, 1979; pp. 505–566.
- ⁷⁹ Mebel, A. M.; Georgievskii, Y.; Jasper, A. W.; Klippenstein, S. J. *Faraday Discuss. Chem. Soc.* 2016, 195, 637–670.
- ⁸⁰ Mebel, A. M.; Georgievskii, Y.; Jasper, A. W.; Klippenstein, S. J. *Proc. Combust. Inst.* 2017, 36, 919–926.

Figure 1

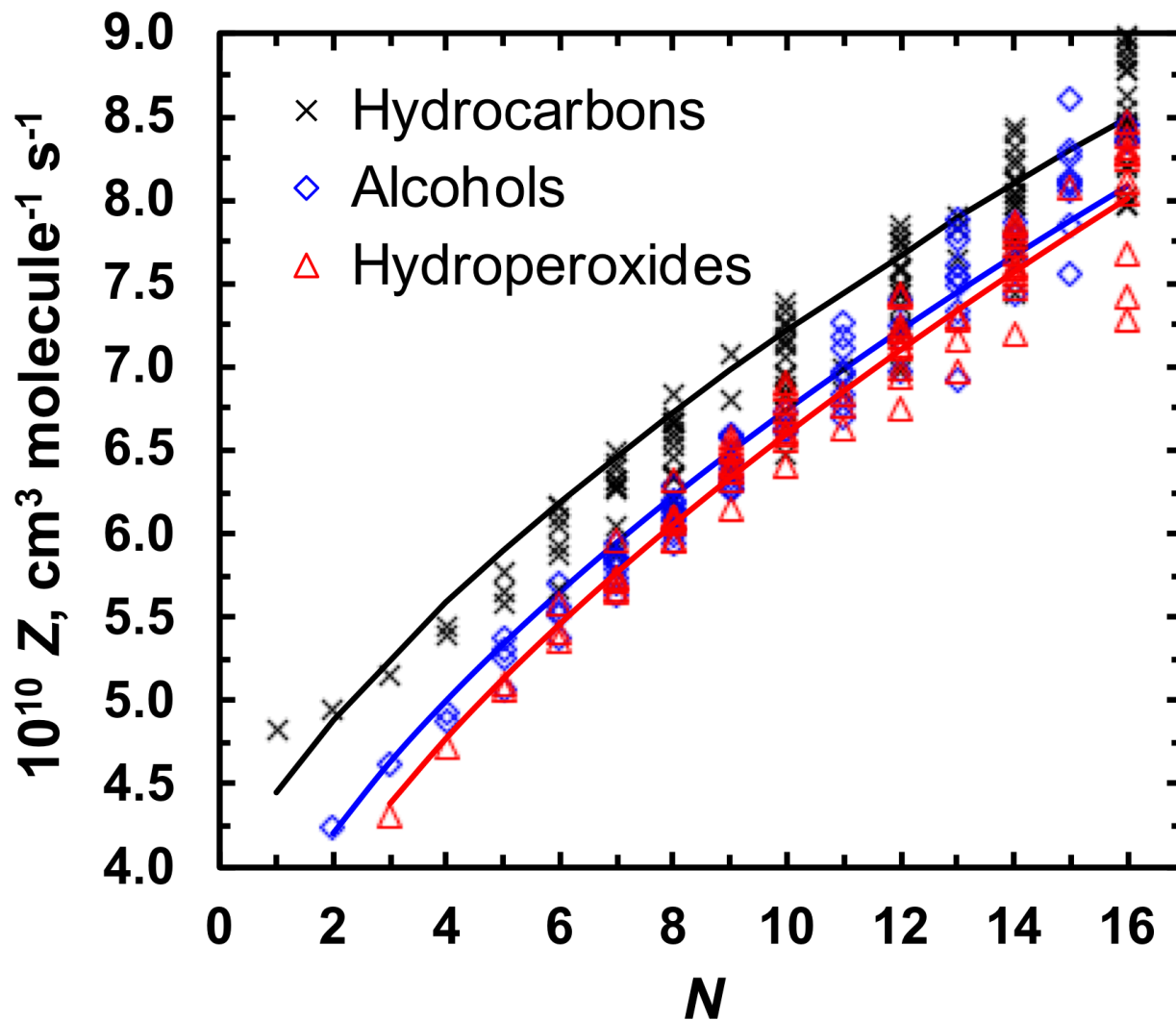


Fig. 1. Computed Lennard–Jones collision rate constants Z at 1000 K and $M = \text{Ar}$ for several hydrocarbons (x), alcohols (diamonds), and hydroperoxides (triangles) and shown as a function of the number of heavy (nonhydrogen) atoms N . Solid lines show the results of the analytic expressions for σ and ε given in the text.

Figure 2

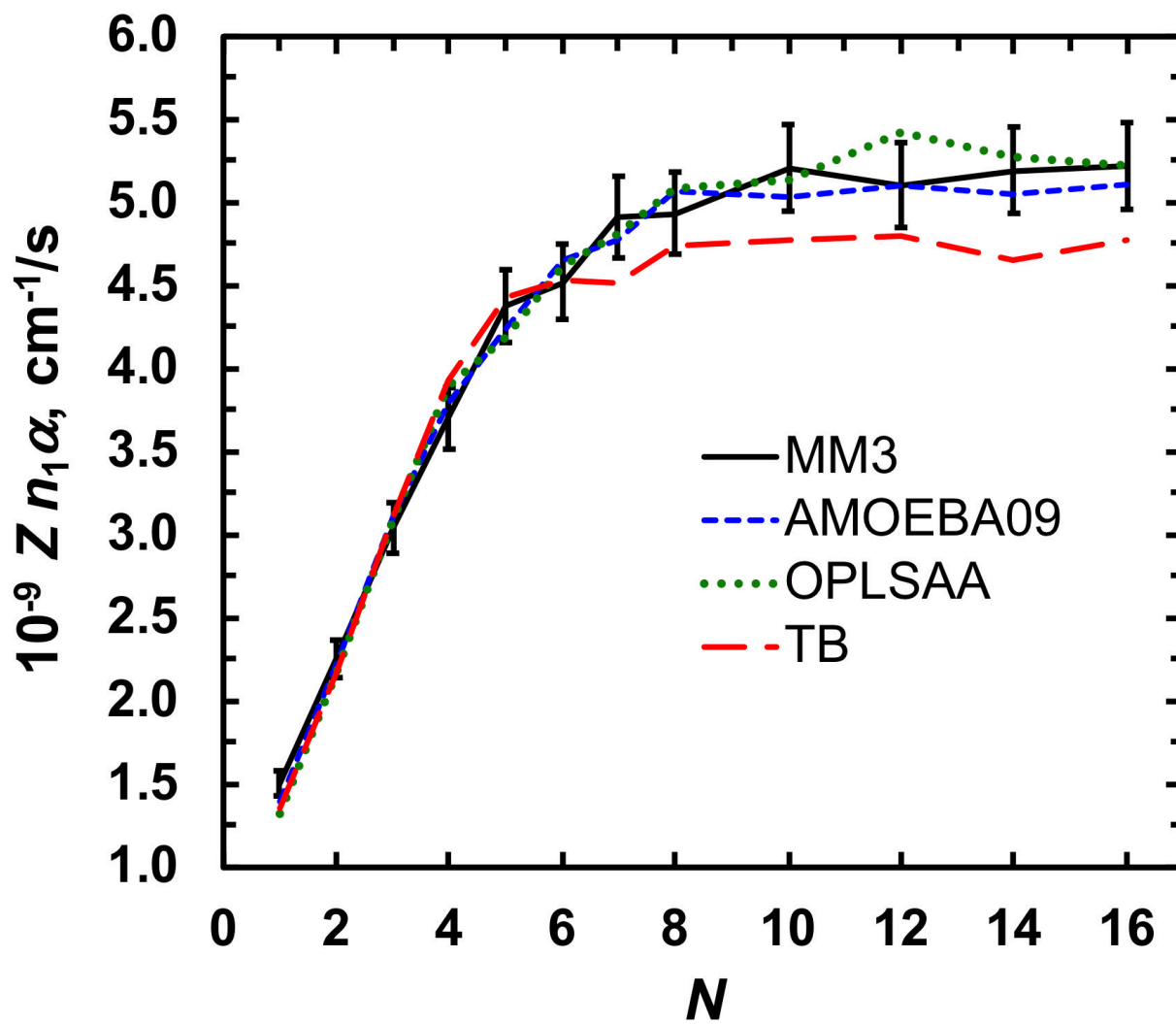


Fig. 2. The deactivating moment of the energy transfer rate constant $Z\alpha$ multiplied by the number density of the bath gas at 1 Torr n_1 for the series of n -alkanes from methane ($N = 1$) to hexadecane ($N = 16$) computed at 1000 K ($n_1 = 9.7 \times 10^{15}$ 1/cm³). Results for four intramolecular potential energy surfaces are shown. The trajectory ensemble sizes used here have 5% 2-sigma statistical uncertainties, as indicated for just one of the curves to reduce clutter.

Figure 3

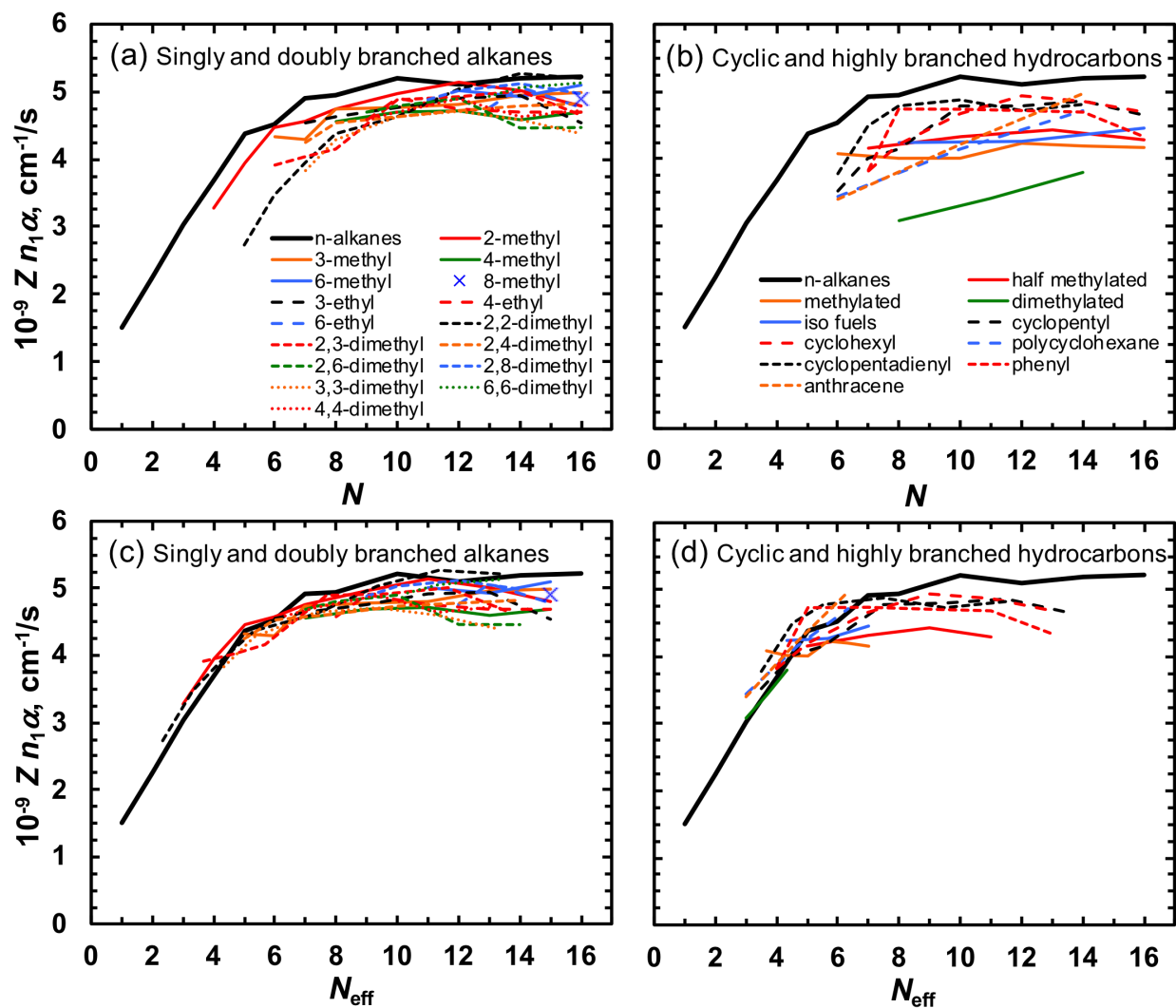


Fig. 3. $Z_{n_1\alpha}$ for several series of (a,c) singly and doubly branched alkanes and (b,d) cyclic and highly branched alkanes and alkenes at 1000 K. The thick black line shows the results for the normal alkane series. Results are shown in (a,b) as a function of the number of heavy atoms N and again in (c,d) as a function of the effective number of heavy atoms N_{eff} .

Figure 4

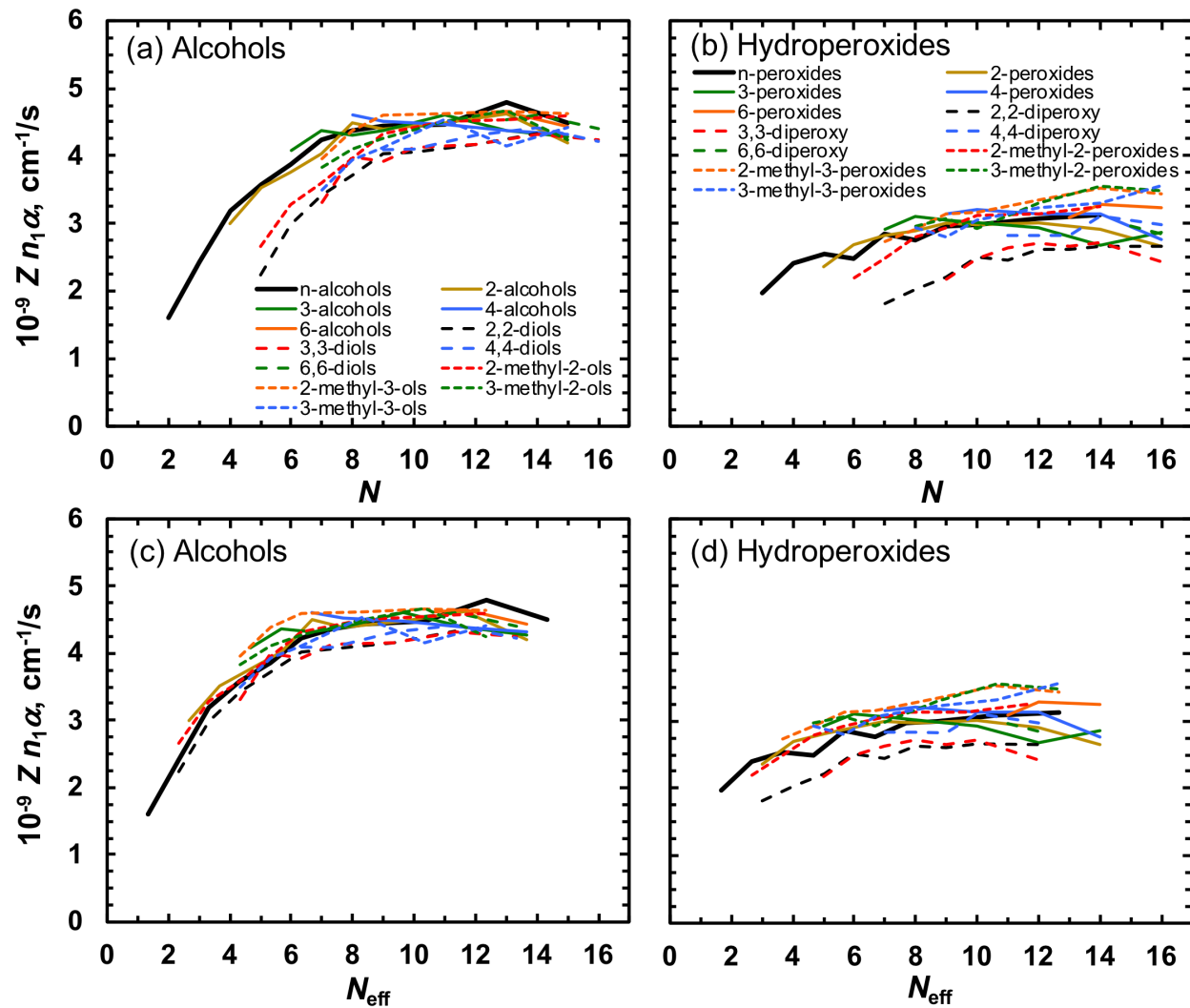


Fig. 4. $Zn_1\alpha$ for several series of (a,c) alcohols and (b,d) hydroperoxides at 1000 K. Results are shown in (a,b) as a function of the number of heavy atoms N and again in (c,d) as a function of the effective number of heavy atoms N_{eff} .

Figure 5

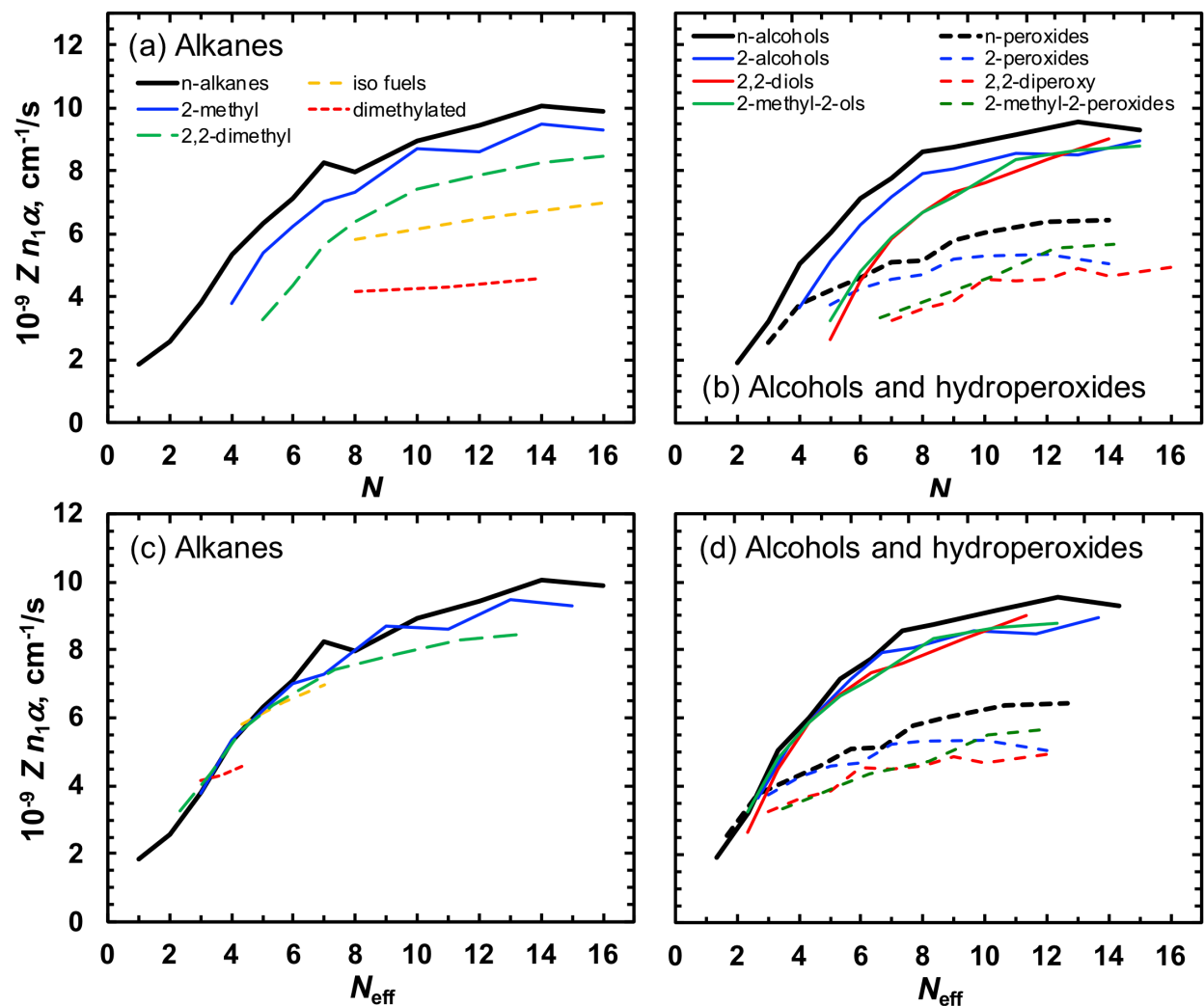


Fig. 5. $Zn_1\alpha$ at 300 K ($n_1 = 3.2 \times 10^{16} \text{ 1/cm}^3$) for (a,c) five series of hydrocarbons and (b,d) eight series of alcohols (solid lines) and hydroperoxides (dashed lines). Results are shown in (a,b) as a function of the number of heavy atoms N and again in (c,d) as a function of the effective number of heavy atoms N_{eff} .

Figure 6

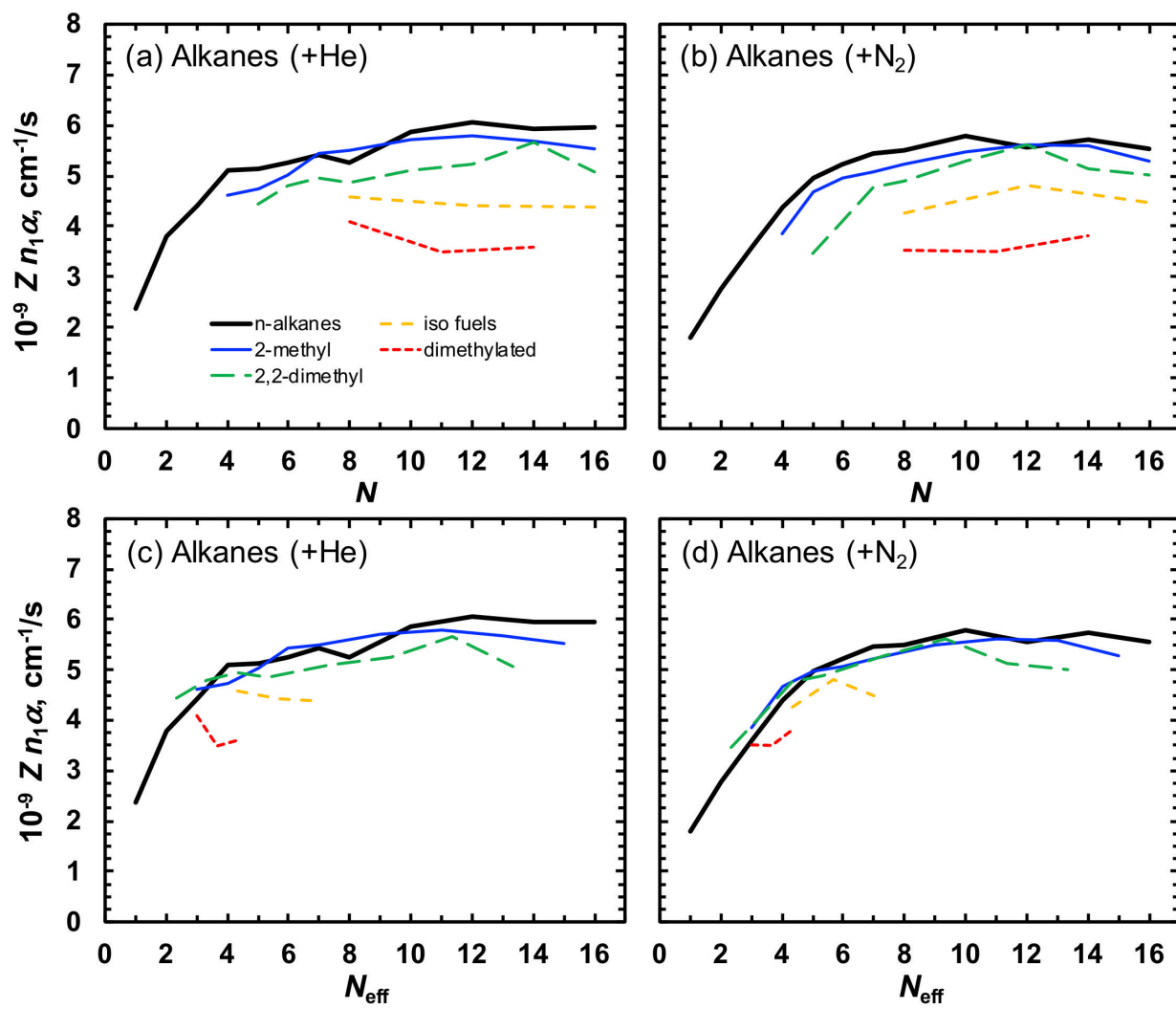


Fig. 6. $Zn_1\alpha$ for five series of hydrocarbons and (a,c) $M = \text{He}$ and (b,d) $M = \text{N}_2$ at 1000 K. Results are shown in (a,b) as a function of the number of heavy atoms N and again in (c,d) as a function of the effective number of heavy atoms N_{eff} .